the FEBS Journal

The subcellular organization of strictosidine biosynthesis in *Catharanthus roseus* epidermis highlights several trans-tonoplast translocations of intermediate metabolites

Grégory Guirimand[1], Anthony Guihur[1], Olivia Ginis[1], Pierre Poutrain[1], François Héricourt[2], Audrey Oudin[1], Arnaud Lanoue[1], Benoit St-Pierre[1], Vincent Burlat[1,*,†] and Vincent Courdavault[1]

1 Université François Rabelais de Tours, EA2106 'Biomolécules et Biotechnologies Végétales', IFR 135 'Imagerie fonctionnelle', Tours, France

2 Université d'Orléans, EA1207 Laboratoire de Biologie des Ligneux et Grandes Cultures, and INRA, USC1328, Arbres et Réponses aux Contraintes Hydriques et Environnementales (ARCHE), Orléans, France

Keywords
alkaloid; bimolecular fluorescence complementation; *Catharanthus roseus*; methyltransferase; strictosidine

Correspondence
V. Courdavault, Université de Tours – EA2106 'Biomolécules et Biotechnologies Végétales', UFR des Sciences et Techniques, 37200 Tours, France
Fax: +33 247 27 66 60
Tel: +33 247 36 69 88
E-mail: vincent.courdavault@univ-tours.fr

Present addresses
*Université de Toulouse, UPS, UMR 5546, Surfaces Cellulaires et Signalisation chez les Végétaux, Castanet-Tolosan, France
†CNRS, UMR 5546, Castanet-Tolosan, France

(Received 5 October 2010, revised 2 December 2010, accepted 16 December 2010)

doi:10.1111/j.1742-4658.2010.07994.x

Catharanthus roseus synthesizes a wide range of valuable monoterpene indole alkaloids, some of which have recently been recognized as functioning in plant defence mechanisms. More specifically, in aerial organ epidermal cells, vacuole-accumulated strictosidine displays a dual fate, being either the precursor of all monoterpene indole alkaloids after export from the vacuole, or the substrate for a defence mechanism based on the massive protein cross-linking, which occurs subsequent to organelle membrane disruption during biotic attacks. Such a mechanism relies on a physical separation between the vacuolar strictosidine-synthesizing enzyme and the nucleus-targeted enzyme catalyzing its activation through deglucosylation. In the present study, we carried out the spatial characterization of this mechanism by a cellular and subcellular study of three enzymes catalyzing the synthesis of the two strictosidine precursors (i.e. tryptamine and secologanin). Using RNA *in situ* hybridization, we demonstrated that loganic acid *O*-methyltransferase transcript, catalysing the penultimate step of secologanin synthesis, is specifically localized in the epidermis. A combination of green fluorescent protein imaging, bimolecular fluorescence complementation assays and yeast two-hybrid analysis enabled us to establish that both loganic acid *O*-methyltransferase and the tryptamine-producing enzyme, tryptophan decarboxylase, form homodimers in the cytosol, thereby preventing their passive diffusion to the nucleus. We also showed that the cytochrome P450 secologanin synthase is anchored to the endoplasmic reticulum via a N-teminal helix, thus allowing the production of secologanin on the cytosolic side of the endoplasmic reticulum membrane. Consequently, secologanin and tryptamine must be transported to the vacuole to achieve strictosidine biosynthesis, demonstrating the importance of trans-tonoplast translocation events during these metabolic processes.

Abbreviations
BiFC, bimolecular fluorescence complementation; CFP, cyan fluorescent protein; ER, endoplasmic reticulum; G10H, geraniol 10-hydroxylase; GFP, green fluorescent protein; GUS, β-glucuronidase; IPAP, internal phloem-associated parenchyma; LAMT, loganic acid *O*-methyltransferase; –LW, leucine-trytophan lacking medium; –LWH, leucine-trytophan-histidine lacking medium; MEP, 2-C-methyl-D-erythritol 4-phosphate; MIA, monoterpene indole alkaloid(s); pGAD, GAL4 activation domain; pLex, LexA DNA-binding domain; SLS, secologanin synthase; SGD, strictosidine β-D-glucosidase; STR, strictosidine synthase; TDC, tryptophan decarboxylase; YFP, yellow fluorescent protein.

Structured digital abstract

- MINT-8080228: *TDC* (uniprotkb:P17770) *physically interacts* (MI:0915) with *TDC* (uniprotkb:P17770) by *two hybrid* (MI:0018)
- MINT-8080246: *LAMT* (uniprotkb:B2KPR3) *physically interacts* (MI:0915) with *LAMT* (uniprotkb:B2KPR3) by *two hybrid* (MI:0018)
- MINT-8080351: *LAMT* (uniprotkb:B2KPR3) and *LAMT* (uniprotkb:B2KPR3) *physically interact* (MI:0915) by *bimolecular fluorescence complementation* (MI:0809)

Introduction

The monoterpene indole alkaloids (MIA) represent more than 2000 structurally and pharmacologically diverse compounds, including valuable molecules such as the antineoplastic vinblastine and vincristine or the antiarrythmic ajmaline [1]. Although their precise functions *in planta* are still poorly characterized, accumulating evidence supports a role for these molecules in plant defence against predators. Such a role has recently been demonstrated in *Catharanthus roseus* (Madagascar periwinkle) [2,3]. Because of their economical importance, numerous studies have focused on the characterization of the MIA biosynthesis in *C. roseus* and, to a lesser extent, in *Rauvolfia serpentina* [1,4]. MIA originate from the condensation of the indole precursor tryptamine with the monoterpene-secoiridoid precursor secologanin (Fig. 1). Tryptamine is a shikimate-derived product generated via the decarboxylation of tryptophan catalyzed by tryptophan decarboxylase (TDC; EC 4.1.1.28) [5]. Secologanin biosynthesis is a more complex process where the methyl-D-erythritol 4-phosphate (MEP) pathway-derived monoterpenoid precursor geraniol is engaged in the monoterpene secoiridoid pathway to produce secologanin [6] (Fig. 1). Among the seven enzymatic reactions putatively involved in the monoterpene secoiridoid pathway, only three enzymes have been characterized at both the molecular and biochemical levels, namely geraniol 10-hydroxylase (G10H; CYP76B6; EC 1.14.14.1), secologanin synthase (SLS; CYP71A1; EC 1.3.3.9) and loganic acid *O*-methyltransferase (LAMT, EC 2.1.1.50). G10H and SLS catalyze the first and last step of the monoterpene secoiridoid pathway, respectively [7,8], and LAMT, which has been characterized recently, catalyzes the penultimate step of this pathway [9] (Fig. 1). The condensation of tryptamine and secologanin is catalyzed by strictosidine synthase (STR; EC 4.3.3.2) [10]. This reaction results in the formation of the first MIA, strictosidine, which is subsequently deglucosylated by strictosidine β-D-glucosidase (SGD; EC 3.2.1.105) [11] to generate an unstable aglycon, leading to the biosynthesis of the numerous MIA subtypes, including vindoline and catharanthine, the two precursors of the pharmaceutically valuable dimeric MIA vinblastine.

Furthermore, at both cellular and subcellular levels, the complex architecture of the MIA biosynthetic pathway has emerged as an important regulatory mechanism in MIA biosynthesis. The high degree of compartmentalization of both gene expression and enzymatic reactions suggests that multiple translocations of biosynthetic intermediates between tissues and/or organelles occur within the cells. Indeed, at the cellular level, the specific detection of the gene products by RNA *in situ* hybridization and, to some extent, by immunolocalization reveals that the biosynthesis of secologanin is initiated in the internal phloem-associated parenchyma (IPAP) cells, at least until the hydroxylation of geraniol by G10H [12–14]. Subsequently, the epidermis houses the reactions catalyzed by SLS, TDC, STR, SGD and two additional enzymes catalyzing the first two steps of vindoline biosynthesis [2,8,15–17]. Finally, the specialized laticifer and idioblast cells constitute the cellular compartment where the final two steps of vindoline biosynthesis are carried out [17]. In addition, on the basis of expressed sequence tag enrichment, LAMT has been proposed to be an epidermis-located enzyme [9]. At the subcellular level, an *in situ* characterization of the localization of MIA biosynthetic enzymes using green fluorescent protein (GFP) and bimolecular fluorescence complementation (BiFC) imaging has also been initiated, with the aim of studying the architecture of the whole MIA biosynthetic pathway and re-evaluating the contradictory results obtained by organelle fractionation on density gradients. Using this strategy, the MEP pathway enzyme hydroxymethylbutenyl 4-diphosphate synthase (EC 1.17.7.1) has been localized to plastids/stromules and G10H has been identified as an endoplasmic reticulum (ER)-anchored cytochrome P450 instead of a (pro-)vacuolar protein [18]. The same strategy was recently used to obtain a complete spatial model of the vindoline pathway [15]. Moreover,

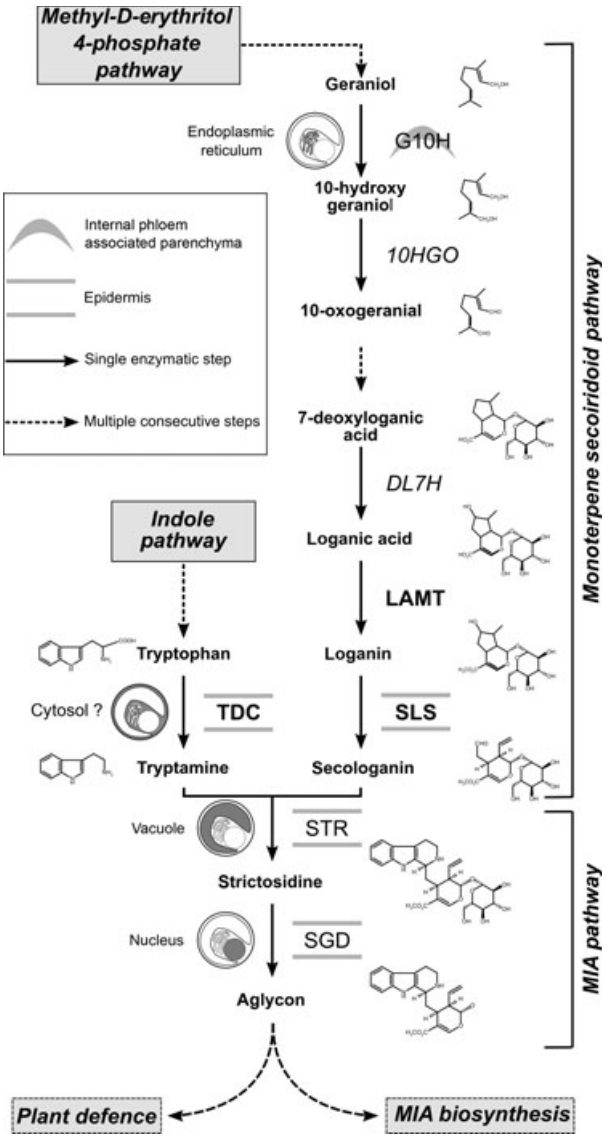

Fig. 1. Biosynthetic pathway of MIA in *C. roseus* cells showing the cellular and subcellular enzyme compartmentalizations. Solid lines represent a single enzymatic step, whereas dashed lines indicate multiple enzymatic steps. The cellular distribution pattern of gene transcripts is indicated by a symbol associated with the name of the enzyme. The protein subcellular localization is indicated next to the enzyme name using grey shading of the compartment within the symbolized cells. The presence of a question mark indicates contradictory/incomplete results. The abbreviations of the uncharacterized enzymes and of the enzymes investigated in the present study are shown in italics and bold, respectively. DL7H, deoxyloganic acid 7-hydroxylase; 10HGO, 10-hydroxygeraniol oxidoreductase.

for both *C. roseus* and *R. serpentina* enzymes, the physical separation between STR and SGD located in the vacuole and the nucleus, respectively, was recently demonstrated [2], leading to a re-evaluation of the previously proposed localization of SGD to the ER [11]. On the basis of this unusual protein distribution, a so-called 'nuclear time bomb' specific mechanism of vacuole-to-nucleus strictosidine activation has been proposed to act as a potential defence process in strictosidine-accumulating *Apocynaceae* [2]. In a continuing effort to characterize the spatial architecture of the MIA biosynthetic pathway using the same strategies, the present study reports on the subcellular organization and possible protein interaction of TDC, LAMT and SLS, comprising the three enzymatic steps preceding the biosynthesis of the first MIA strictosidine within the epidermis. This led us to establish a complete scheme of strictosidine biosynthesis in epidermal cells, highlighting several orientated trans-tonoplast translocation events of metabolic intermediates, and allowing both regulation of MIA metabolic flux and a specific protein cross-linking-based mechanism of plant defence.

Results

LAMT is specifically expressed in the epidermis of *C. roseus* aerial organs and shows an expression profile in cultured cells similar to other MIA-related epidermis-specific genes

According to expressed sequence tag enrichment in a leaf epidermis-enriched *C. roseus* cDNA library and a tissue-specific analysis of activity, LAMT has been proposed to be preferentially localized to the epidermis [9]. However, no *in situ* localization data are available to support this result compared to TDC, SLS, STR and SGD, for which corresponding gene products have been localized to the epidermis by RNA *in situ* hybridization and/or immunolocalization. To address this issue, the distribution of *LAMT* transcripts has been analyzed using the same approach in cotyledons of *C. roseus* seedlings and young developing leaves. Using the anti-sense probe, the *LAMT* mRNA was specifically detected in the epidermis of both organs in a similar manner to the *SLS* transcripts used as an epidermis-specific control (Fig. 2). No signal could be observed with the *LAMT* sense probe. This clearly shows that these two consecutive steps essentially occur in the epidermis. In addition, we also carried out a study of the regulation of *LAMT* expression by RT-PCR analysis performed on RNA from *C. roseus* C20D cells. These cells are able to synthesize MIA in response to the depletion of auxin from the culture medium (MIA production condition), whereas the presence of auxin dramatically

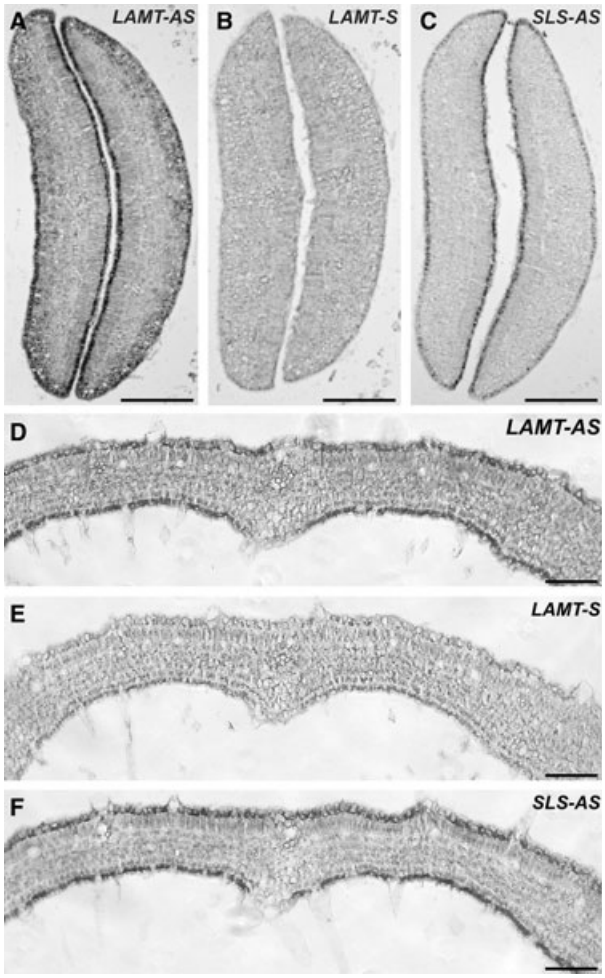

Fig. 2. Epidermis-specific expression of *LAMT* in *C. roseus* cotyledons and young developing leaves. Serial sections of cotyledons (A–C) and young developing leaves (D–F) were hybridized either with *LAMT*-antisense (AS) probes (A, D), with *LAMT*-sense (S) probes (B, E) used as a negative control or with *SLS*-AS (C, F) probes used as a positive control. Scale bar = 100 μm.

inhibits this biosynthesis (cell maintenance condition) [19]. Under both conditions, *LAMT* and *SLS* display a similar pattern of expression, being gradually expressed with a maximum reached at the end of the cell culture (day 7), whereas IPAP-expressed *G10H* is strongly down-regulated in cell maintenance conditions and up-regulated during MIA production conditions (Fig. 3), as reported previously [14]. This result suggests that, in a similar manner to the other MIA-related epidermis-specific genes, *LAMT* expression is not rate-limiting during MIA biosynthesis, in contrast to earlier steps in monoterpenoid biosynthesis encoded by IPAP-specific genes, such as MEP pathway genes and *G10H* [14].

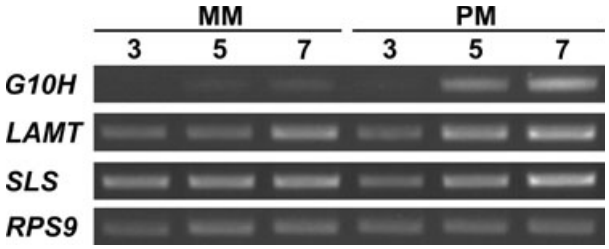

Fig. 3. RT-PCR analysis of expression of *G10H*, *LAMT* and *SLS* in *C. roseus* cells. C20D cells cultured in either maintenance medium (MM) in presence of 2,4-dichlorophenoxyacetic acid or in MIA production medium (PM) in the absence of 2,4-dichlorophenoxyacetic acid were harvested after 3, 5 and 7 days of subculture before RNA extraction and reverse transcription. The resulting cDNAs were subjected to semi-quantitative PCR using the specific *G10H*, *LAMT* and *SLS* primers. The expression of *RPS9* that encodes the 40S ribosomal protein was used as a control.

TDC is localized to the cytosol and is organized as a homo-oligomer *in vivo*

To complete the characterization of the subcellular organization of the epidermis-located steps of MIA biosynthesis, we analyzed the subcellular localization of TDC using the transient expression of GFP-fusion proteins within *C. roseus* cells. Independent of the orientation of the fusion with GFP, both TDC-GFP and GFP-TDC remained cytosolic, as illustrated by a perfect merging of fluorescence with the mcherry-β-glucuronidase (GUS) cytosolic marker (Fig. 4A–D), exclusion from the nucleus (Fig. 4E–H) and an absence of merging with the nuclear sub-signal of the mcherry nucleocytosolic marker (Fig. 4I–L). Additionally, no merging of the fluorescence signals of TDC-GFP and cell wall could be observed after staining cellulose with calcofluor (Fig. 4M–P). This suggests that TDC is exclusively cytosolic, in agreement with the absence of known targeting sequences within the protein sequence, based on bioinformatic analysis using different software (data not shown).

To study the *in vivo* oligomerization state of TDC, BiFC assays were conducted in *C. roseus* cells. For such an analysis, the TDC coding sequence was fused either to the N-terminal (YFP^N) or C-terminal (YFP^C) fragments of yellow fluorescent protein (YFP) at both their N- or C-terminal end to produce TDC-YFP^N, TDC-YFP^C, YFP^N-TDC and YFP^C-TDC, respectively. During co-transformation experiments, the different combinations of these constructs all lead to the formation of a BiFC complex, as revealed by the observation of a yellow fluorescence within the cells (Fig. 5A–H). This signal perfectly merged with the fluorescence of the cyan fluorescent protein (CFP)-GUS cytosolic marker,

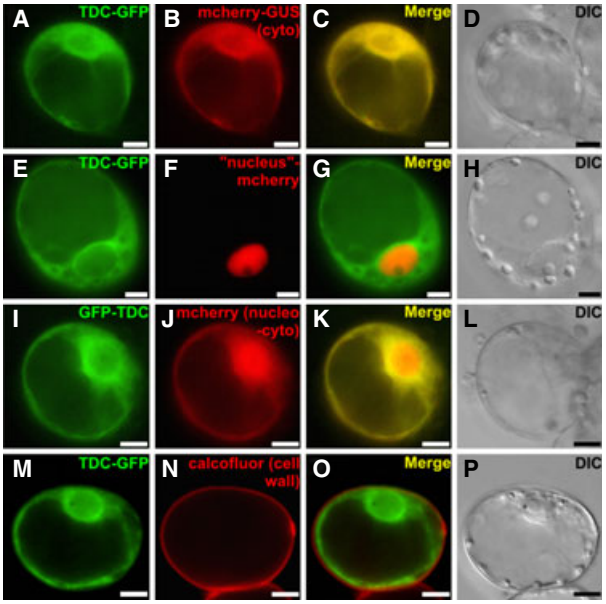

Fig. 4. Cytosolic localization of TDC in *C. roseus* cells. Cells were transiently transformed with TDC-GFP (A–H, M–P) or GFP-TDC (I–L) expressing vectors in combination with either the cytosolic (cyto) mcherry-GUS (A–D), the nucleus-mcherry (E–H), the nucleo-cytosolic (nucleocyto) mcherry (I–L) markers or with a calcofluor cell wall staining (M–P). Co-localization of the two fluorescence signals are shown in the merged image (C, G, K, O). The morphology was observed by differential interference contrast (DIC) microscopy. Scale bar = 10 μm.

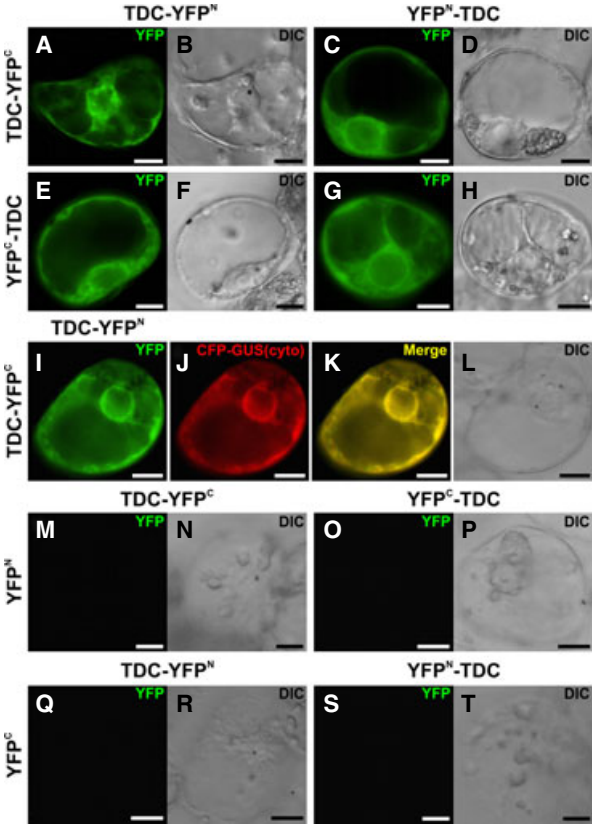

Fig. 5. Analysis of TDC oligomerization in *C. roseus* cells using BiFC assays. (A–H) Cells were co-transformed using a combination of plasmids as indicated at the top (fusion with the YFP^N fragment) and on the left (fusion with the YFP^C fragment). For the TDC-YFP^N/TDC-YFP^C combination, an additional co-transformation was performed with the CFP-GUS cytosolic (I–L) marker. In addition, co-transformations with BiFC empty vectors were also performed to check the specificity of the interactions (M–T). The morphology was observed by differential interference contrast (DIC) microscopy. Scale bar = 10 μm.

as shown for the TDC-YFP^N and TDC-YFP^C combination (Fig. 5I–L). By contrast, no YFP reconstitution could be visualized when co-expressing the fusion proteins with nonfused YFP^N and YFP^C fragments, thereby validating the specificity of the TDC oligomerization in *C. roseus* cells (Fig. 5M–T). To further validate this *in vivo* interaction, we used an independent experimental approach by performing a yeast two-hybrid system analysis. Co-transformation of yeast with the prey construct carrying the fusion of GAL4 activation domain (pGAD) with TDC and the bait construct harbouring the fusion of LexA DNA-binding domain (pLex) with TDC allowed the recovery of yeast growth on selective medium and the acquirement of β-galactosidase activity indicating a strong protein–protein interaction (Fig. 6 and Table 1). No yeast growth was observed when pGAD-TDC or pLex-TDC were expressed with pLex or pGAD alone, or with pGAD-LAMT or pLex-LAMT, used as negative controls, demonstrating the specificity of the TDC self-interaction (Fig. 6 and Table 1). Taken together, these results indicate that TDC forms homo-oligomers *in vivo* and remains exclusively cytosolic within *C. roseus* cells.

LAMT is also localized to the cytosol and organized as a homo-oligomer *in vivo*

We carried out a similar approach to study the LAMT subcellular localization and *in vivo* protein interaction. Primary sequence analysis of LAMT using bioinformatic software did not reveal any targeting motif within the protein (data not shown). We transiently expressed the YFP-fusion protein in both orientations (LAMT-YFP or YFP-LAMT) in *C. roseus* cells to avoid the possible masking of an unidentified localization motif at the N- or C-terminal end of LAMT. Both fusion proteins displayed a nucleocytosolic fluorescence signal, as demonstrated by the co-localization with the signal of the co-expressed CFP nucleocytosolic marker (Fig. 7A–H). BiFC analysis also revealed

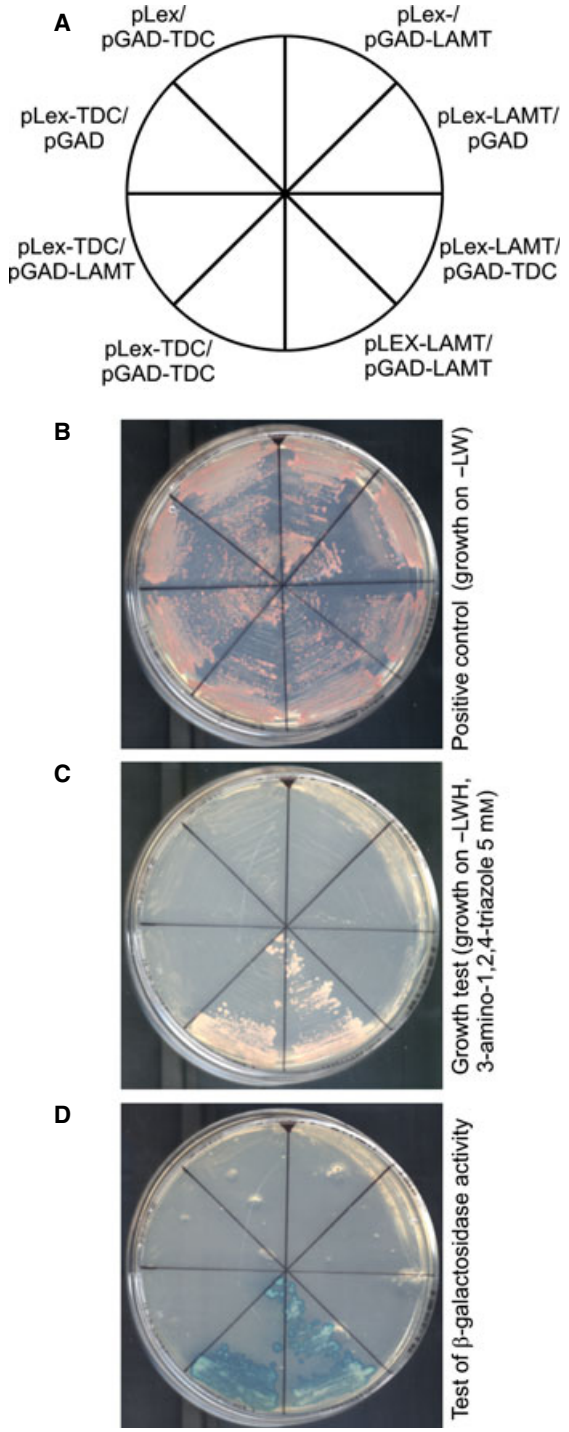

Fig. 6. Analysis of TDC and LAMT interactions by yeast two-hybrid experiments. (A) Schematic representation of co-transformant yeast streaks. (B) Growth of positive controls on –LW. (C) Growth test on –LWH, including 5 mM 3-amino-1,2,4,triazole allowing the identification of the protein interactions. (D) Test of β-galactosidase activity allowing the confirmation of protein interactions and the evaluation of the strength of protein interactions.

Table 1. Analysis of TDC and LAMT interaction using yeast two-hybrid assays. + and – symbolize an interaction and no interaction between the partners, respectively. The number of '+'signs is proportional to the intensity of the interaction.

	pLex-TDC	pLex-LAMT	pLex
pGAD-TDC	+++	–	–
pGAD-LAMT	–	++	–
pGAD	–	–	–

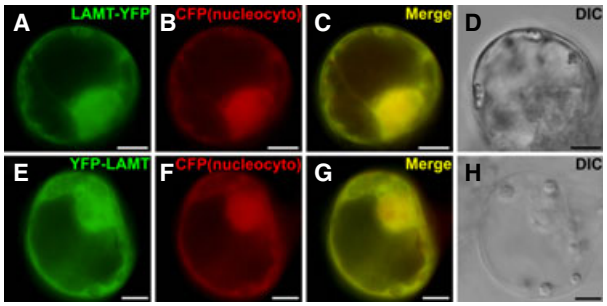

Fig. 7. Nucleocytosolic localization of LAMT in *C. roseus* cells. Cells were transiently transformed with LAMT-YFP (A–D) or YFP-LAMT (E–H) expressing vectors in combination with the nucleocytosolic (nucleocyto) CFP marker. Co-localization of the two fluorescence signals are shown in the merged image (C, G). The morphology was observed by differential interference contrast (DIC) microscopy. Scale bar = 10 μm.

that LAMT is able to form homo-oligomers in *C. roseus* cells regardless of the combination of the fusion proteins (Fig. 8A–H). As observed for the TDC constructs, no BiFC complex reconstitution was visualized when co-expressing the fusion proteins with non-fused YFP^N and YFP^C fragments used as negative controls (data not shown). The formation of LAMT oligomers was also confirmed by a yeast two-hybrid system analysis as well as the specificity of interaction because no growth of transformants was observed in experiments testing the LAMT–TDC cross-interactions (Fig. 6 and Table 1). Interestingly, an analysis of the distribution of the BiFC complex *in vivo* revealed the restriction of the proteins to the cytosol as well as their exclusion from the nucleus (Fig. 8I–L) in contrast to the nucleocytosolic localization of LAMT-YFP and YFP-LAMT (Fig. 7A–H). This indicates that oligomerization of LAMT within the cytosol prevents its passive diffusion to the nucleus in *C. roseus* cells.

SLS is a cytochrome P450 anchored to the endoplasmic reticulum by an N-terminal helix

To complete the characterization of the compartmentalization of secologanin biosynthesis, we studied the

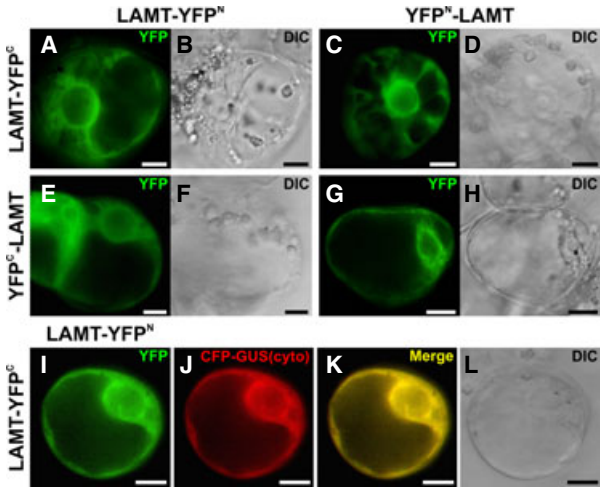

Fig. 8. Analysis of LAMT homodimerization in *C. roseus* cells using BiFC assays. (A–H) Cells were co-transformed using a combination of plasmids as indicated at the top (fusion with the YFP^N fragment) and on the left (fusion with the YFP^C fragment). For the LAMT-YFP^N/LAMT-YFP^C combination, an additional co-transformation was performed with the CFP-GUS cytosolic marker (I–L). The morphology was observed by differential interference contrast (DIC) microscopy. Scale bar = 10 μm.

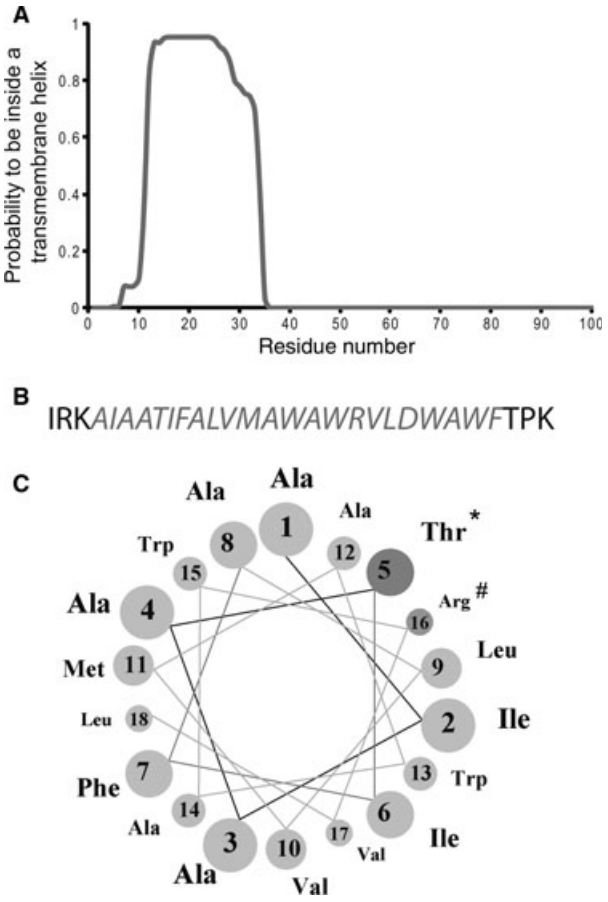

Fig. 9. Detection of a putative transmembrane helix at the N-terminal end of SLS. (A) Probability for a residue to be inside a transmembrane helix as calculated for the first 100 residues of SLS with a Markov model by the TMHMM server (http://www.cbs.dtu.dk/services/TMHMM/). (B) The sequence of the putative transmembrane helix is shown in italics. (C) Projection of the predicted helical wheel represented as a cross-sectional view of the axis using a device available at http://cti.itc.virginia.edu/~cmg/Demo/wheel/wheelApp.html. Polar (*) and basic (#) residues are indicated by the respective symbols, whereas nonpolar residues do not have any sign.

subcellular localization of SLS, which catalyzes the last step of this pathway. SLS is one of the cytochrome P450s involved in the MIA biosynthetic pathway that has not been localized at the subcellular level, in contrast to tabersonine 16-hydroxylase (T16H; CYP71D12; EC 1.14.13.73) and G10H, which have both been localized to the ER [15,18,20]. Bioinformatic sequence analysis of SLS led to the identification of a putative 23-residue transmembrane N-terminal helix (residues 11–33) (Fig. 9). To ensure the accessibility of this sequence in our GFP imaging approach, we transiently expressed a SLS-GFP fusion protein in *C. roseus* cells. The transformed cells displayed a GFP fluorescence signal surrounding the nucleus and perfectly co-localizing with the 'ER'-mcherry marker signal (Fig. 10A–H), indicating that SLS is specifically localized to the ER. In a small number of transiently transformed cells, we also observed the labelling of ER globular structures typical of organized smooth ER (data not shown). In addition, fusion and deletion experiments revealed that the predicted transmembrane helix is necessary and sufficient for SLS localization to the ER because its fusion to GFP (thSLS-GFP, SLS residues 1–33) led to an ER localization (Fig. 10I–L), whereas its deletion from SLS (ΔthSLS, SLS residues 34–524) caused a loss of ER targeting (Fig. 10M–P). In such cases, the ΔthSLS fusion protein formed punctuated aggregates in the cytosol in close vicinity with plastids, as described previously for the transmembrane helix truncated variant of G10H [18].

Discussion

Subsequent to the first studies of enzymes localization *in planta*, the compartmentalization of secondary metabolite biosynthetic pathways at both the cellular and subcellular levels and the resulting inter- and intracellular molecule translocations have emerged as highly complex processes giving rise to several regulatory mechanisms of metabolite biosynthesis and/or

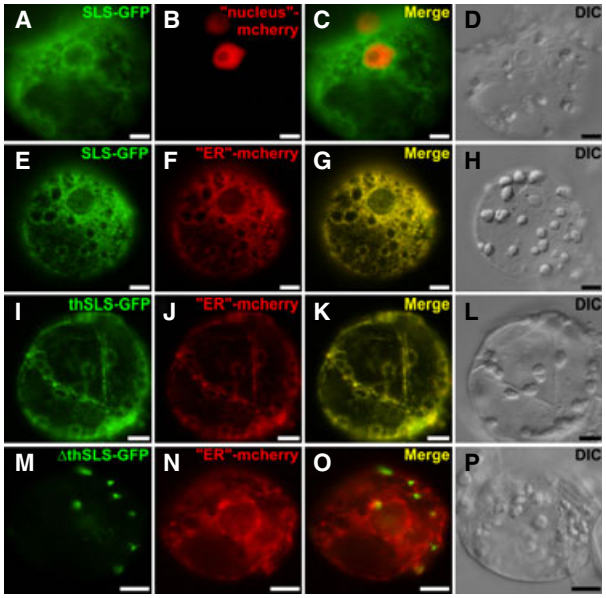

Fig. 10. ER anchoring of SLS and functional characterization of the N-terminal transmembrane helix in *C. roseus* cells. Cells were transiently transformed with SLS-GFP (A–H), thSLS-GFP (I–L) or ΔthSLS-GFP (M–P) expressing vectors in combination with different markers as mentioned on the images of the first two columns. Co-localization of the two fluorescence signals is shown in the merged image. The morphology was observed by differential interference contrast (DIC) microscopy. th, transmembrane helix; Δth, absence of the th; nucleocyto, nucleocytosol. Scale bar = 10 μm.

plant defence [21]. Accordingly, *C. roseus* displays one of the most elaborated biosynthetic pathways *in folio* with at least four cell types involved in MIA production, including the parenchyma of internal phloem, epidermis, laticifers and the idioblasts [1,4,22]. In addition, the spatial sequestration, at the subcellular level, of STR in the vacuole and SGD in the nucleus of leaf epidermal cells led to the development of a plant defence system mediated by protein cross-linking and based on the SGD-mediated massive deglucosylation of strictosidine, subsequent to organelle membrane disruption during herbivore and necrophytic microorganism attacks [2]. This sheds light on the pivotal role of the epidermis as the first barrier within defence processes and in secondary metabolism [2,23], even though the whole architecture of the strictosidine biosynthetic pathway has not yet been elucidated in this tissue. In the present study, we investigated the subcellular distribution and the oligomerization state of the three other epidermis-localized strictosidine biosynthetic steps catalyzed by TDC, LAMT and SLS.

LAMT has been proposed to be an epidermis-localized step of MIA biosynthesis, primarily on the basis of its cloning and discovery within a leaf epidermis-enriched cDNA library [9]. To validate such a hypothesis, we studied the distribution of the *LAMT* transcripts in cotyledons and young developing leaves of *C. roseus* by RNA *in situ* hybridization. As expected, *LAMT* mRNAs were specifically detected in both the abaxial and adaxial epidermis of cotyledons and leaves, as previously observed for *SLS* transcripts (Fig. 2). This result confirms that LAMT is a component of the epidermis-specific pool of enzymes involved in the intermediate steps of MIA biosynthesis, which so far include SLS [8], TDC, STR [17], SGD [2] and 16-hydroxytabersonine 16-*O*-methyltransferase (EC 2.1.194) [15]. This reinforces the pivotal role of the epidermis in MIA and other secondary metabolite biosynthetic pathways such as flavanoids, indoles and/or secoiridoid-monoterpenes [23]. The epidermis-specific expression of these genes also suggests that no intercellular translocations of biosynthetic intermediates should occur to regulate MIA biosynthesis or participate in plant defence processes within these central steps of the MIA pathway (Fig. 1). In turn, it also indicates that the metabolite transported from IPAP to the epidermis is further transformed after G10H and before loganic acid biosynthesis, as previously proposed (Fig. 1) [9]. In addition, the similar pattern of gene expression of both *LAMT* and *SLS* in *C. roseus* cells (Fig. 3) also reinforces the previously proposed notion of tissue-reminiscent regulation of gene expression in C20D undifferentiated cell cultures [14]. Such a model includes an auxin-mediated inhibition of the genes expressed in IPAP cells of leaves as demonstrated by the rate-limiting effect of *G10H*, whereas genes expressed in the leaf epidermis are not auxin-sensitive and are not rate-limiting MIA biosynthetic genes.

Next, we characterized the subcellular localization and oligomeric organization of TDC, LAMT and SLS, aiming to complement the current map of MIA-biosynthetic enzyme compartmentalization within the epidermis [2,15]. Using biolistic-mediated transient transformations and GFP imaging, we showed that TDC accumulated in the cytosol irrespective of the orientation of the fusion in *C. roseus* cells (Fig. 4). This is in agreement with previous results obtained by density gradient analysis [24]. However, no targeting of TDC to the cell wall was observed (Fig. 4M–P), in contrast to the unexpected immunolocalization of TDC in the apoplastic zone of *C. roseus* hairy roots [25]. This cytosolic localization correlates with the absence of targeting signal within the primary sequence of TDC, based on bioinformatic analysis, as was also hypothesized to hold true for the first 13 residues of the protein that are truncated in the *C. roseus* cell-purified TDC

[26,27]. In addition, both BiFC and yeast two-hybrid assays established that TDC occurs as homo-oligomers *in vivo* (Figs 5 and 6) in agreement with purification experiments [28–31]. On the basis of these experiments that allowed the purification of a 110 kDa protein, as well as the molecular weight of the TDC monomer (55 kDa), it could be hypothesized that TDC occurs at least as homo-dimers *in vivo*. Our findings thus represent the first *in situ* demonstration of the oligomerization of TDC within the cytosol of *C. roseus* cells (Fig. 5). Such formation of homodimers, whose predicted size reached 110 kDa, could prevent the passive diffusion of the TDC monomer to the nucleus because the upper limit of nuclear pores is no larger than 60 kDa [32], thus restricting the tryptamine decarboxylation to the cytosol (Fig. 11).

Using GFP fusion proteins, we also showed that LAMT displayed a nucleocytosolic localization for both LAMT-YFP and YFP-LAMT fusion proteins, thus ruling out the possibility of masking any, yet to be identified, putative N-terminal or C-terminal targeting signal within the fusion protein (Fig. 7). Furthermore, by combining BiFC and yeast two-hybrid assays, we demonstrated that LAMT forms homo-oligomers in *C. roseus* cells (Figs 6 and 8). This is in agreement with the findings indicating that several other members of the salicylic acid methyltransferase/benzoic acid methyltransferase/theobromine synthase family of carboxylmethyltransferases, whose 3D structures have been characterized, form homodimers [33–35], supporting the view that LAMT also forms a homodimer. In addition, the crystallization of the *Clarkia breweri* salicylic acid carboxyl methyltransferase revealed that the homodimer bears proximal N- and C-termini [35]. This could explain why each pair of split-YFP protein could reform BiFC complexes (Fig. 8). Interestingly, in *C. roseus* cells, these BiFC complexes only displayed a cytosol localized fluorescence signal and were excluded from the nucleus. As previously discussed for TDC, such protein homodimerization could prevent the passive diffusion of the LAMT monomer (predicted size of 42 kDa) to the nucleus, inducing in turn the sequestration of the LAMT homodimer (predicted size of

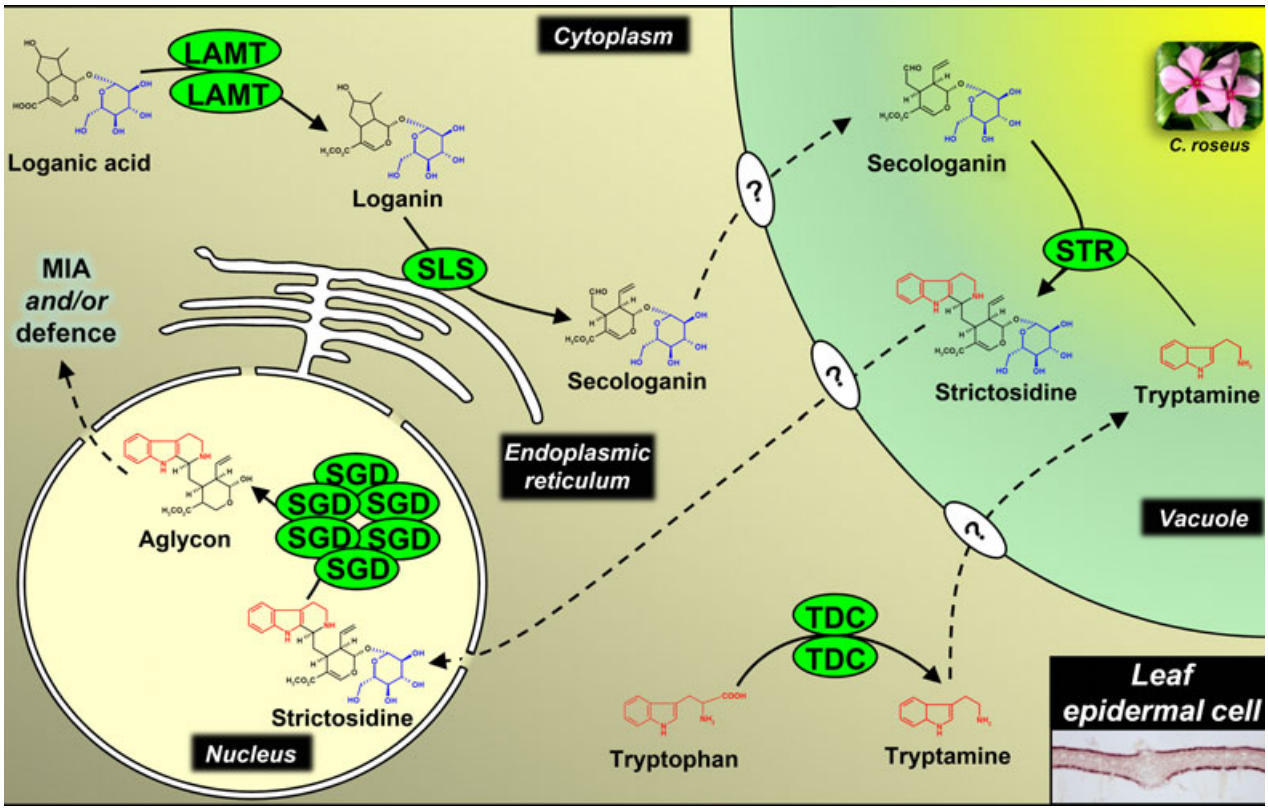

Fig. 11. Spatial model depicting the subcellular organization of the strictosidine biosynthetic pathway in epidermal cell of *C. roseus* leaves. '?' indicates the putative transportation system of tryptamine, secologanin and stricosidine across the tonoplast. The number of repetitions of each enzyme name indicates whether it has been identified as a homodimer (LAMT or TDC) or multimer (SGD).

84 kDa) in the cytosol and therefore restricting loganin synthesis to the cytosol (Fig. 11). These results also highlight the importance of combining distinct analytical approaches when studying the subcellular localization of proteins so as to avoid any misinterpretation of the results obtained, especially for proteins that exhibit a nucleocytosolic localization.

Subsequent to its synthesis within the cytosol, loganin is converted to secologanin by SLS, which has been proposed to operate in or at the vacuole [36,37]. This hypothesis was partially based on the absence of a proline-rich motif ([P/I]Px[P/G]xP) close to the SLS N-terminus, which is considered to be important for the structure of microsomal cytochrome P450 [8,38]. However, the results obtained in the present study clearly establish that SLS is targeted to the ER (Fig. 10), in agreement with the identification of a putative 23-residue transmembrane helix at the N-terminus of the protein (Fig. 9) that is both necessary and sufficient to ensure this targeting. On the basis of the classical model of cytochrome P450 subcellular localization [39], SLS could be anchored to the ER membrane via the N-terminal transmembrane helix to expose the catalytic site to the cytosol (Fig. 11). This suggests that the loganin-to-secologanin conversion operates in the cytosol and not in the vacuole as previously proposed [37]. It cannot be excluded that the labelling of organized smooth ER in some cells could be the consequence of low affinity interactions between the SLS-GFP fusion proteins as a result of over-expression, as described previously for other ER-anchored enzymes [40].

Taken together, the results obtained in the present study allow us to establish an integrated model of the compartmentalization of strictosidine biosynthesis at both cellular and subcellular levels (Fig. 11). Within the epidermal cells of leaves, the final step of the synthesis of the indole precursor of MIA is catalyzed by a TDC homodimer located exclusively in the cytosol with no passive diffusion to the nucleus. Similarly, the penultimate step of the synthesis of the terpenoid precursor is performed by a cytosol-sequestrated LAMT homodimer. The resulting loganin is next converted into secologanin in the same compartment by the ER-anchored SLS. To achieve the production of strictosidine, both precursors are then transported, by as yet uncharacterized mechanisms, into the vacuole where the condensation of tryptamine and secologanin to form strictosidine is carried out by STR, as described previously [2]. Strictosidine is then translocated outside the vacuole to allow its deglucosylation by a multimerized complex of SGD in the nucleus. Depending on the physiological conditions, the resulting aglycon could be engaged either in further steps of MIA biosynthesis or in plant defence mechanisms after the disruption of membranes [2]. Therefore, the tonoplast appears as a crucial site for different directional translocation of at least three intermediate metabolites constituting three potential rate-limiting steps of the metabolic flux in MIA biosynthesis (Fig. 11). The molecular mechanisms underlining these trans-tonoplast translocation events remain to be discovered in *C. roseus* [41]. Recently, an active transport system catalysed by ATP-binding cassette transporters was implicated in the movement of the benzylisoquinoline alkaloid berberine in *Coptis japonica* [42,43]. Such a mechanism may constitute a good candidate for substrate translocation events in *C. roseus*. Finally, the present study highlights the importance of the epidermis as a plant defence barrier, as well as the need to characterize accurately the subcellular compartmentalization of strictosidine biosynthesis when aiming to elucidate the plant defence mechanisms involving alkaloids and to identify the potential critical steps for manipulation (by metabolic engineering) that will enable increased alkaloid production.

Experimental procedures

Transcript analysis by semi-quantitative RT-PCR

The transcriptional regulation of LAMT has been investigated in *C. roseus* cell suspension culture (C20D strain) by semi-quantitative RT-PCR. Seven-day-old cells usually maintained in a 2,4-dichlorophenoxyacetic acid (4.5 μM)-containing medium (maintenance medium) were either subcultured on maintenance medium or in a 2,4-dichlorophenoxyacetic acid-free medium (MIA production medium) and harvested 3, 5 and 7 days after subculture as described previously [44]. Frozen cells were pulverized in liquid nitrogen and total RNA was extracted by the use of the Nucleospin RNA plant kit in accordance with the manufacturer's instructions (Macherey-Nagel, Hoerdt, France). Total RNA (2 μg) was treated with RQ1 RNase-free DNase (Promega, Charbonnières-les-Bains, France) and used for first-strand cDNA synthesis by priming with oligo d(T17) (0.6 μM). Reverse transcription reactions were performed in a 20 μL reaction mixture by use of the iScript™ cDNA synthesis kit (Bio-Rad, Marnes-la-Coquette, France). Two microlitres of each RT reaction were used for subsequent PCR. PCR amplifications using gene-specific primers (a list of the primers used is provided in Table 2) were started with an initial denaturation at 94 °C for 2 min and then performed under the conditions: 94 °C for 30 s, 52 °C for 30 s and 72 °C for 50 s, followed by a final extension at 72 °C for 5 min. The number of cycles was, respectively, 30, 33 and 35 for *RPS9*, *G10H* and both *LAMT* and *SLS* genes. PCR

Table 2. List of primers used in the present study.

Primer	Sequence (5′- to 3′)
G10H-for	TACCAGCCAAGAAAGCCCTGAGG
G10H-rev	AGCCATCCCACCTTCAAGCTTCC
LAMT-for	CATTGGTTATCTAAAGTGCCCA
LAMT-rev	CTTCATGGGATGAGGTAAAGT
RPS9RTfor	AGGCACATAAGGGTTGGAAAG
RPS9RTrev	AGGTCTGATTGATATCCTTCAGT
SLS-for	TGCCGACAGTAATGCTTCACA
SLS-rev	ACACACTAATTCTGGATAGGGCT
TDC-GFPfor	GCACTAGTATGGGCAGCATTGATTCAACAAATGTA
TDC-GFPrev	GCACTAGTAGCTTCTTTGAGCAAATCATCGGTTAATT
LAM-YFPfor	GCACTAGTATGGTTGCCACAATTGATTCCATTG
LAM-YFPrev	GCACTAGTATTTCCCTTGCGTTTCAAGACAAGG
SLS-S	AGCAGATCTTCTAGAAGAAATGGAGATGGATATGGA
SLS-AS	AGCAGATCTCTGCTCTCAAGCTTCTTGTAGATGA
SLS-pep-for	GCAGATCTGATGGAGATGGATATGGATACCA
SLS-pep-rev	GCACTAGTAAACCATGCCCAATCCAACAC
SLS-del-S	GGAGATCTGACTCCTAAGAGGATCGAGAAACGT
SLS-del-AS	GGACTAGTGCTCTCAAGCTTCTTGTAGATGACA
2yeast-LAMfor	GCAGATCTCCATGGTTGCCACAATTGATTCCATTG
2yeast-LAMrev	GCAGATCTCCATTTCCCTTGCGTTTCAAGACAAGG
2yeast-TDCfor	GCAGATCTCCATGGGCAGCATTGATTCAACAAATGTA
2yeast-TDCrev	GCAGATCTCCAGCTTCTTTGAGCAAATCATCGGTTAATT

products (25 μL) were analyzed by electrophoresis on a 1.2% agarose gel.

Bioinformatic sequence analysis

The predictions of protein subcellular localization were performed using SIGNALP 3.0 (http://www.cbs.dtu.dk/services/SignalP/), PSORT (http://psort.ims.u-tokyo.ac.jp/), TARGETP 1.1 (http://www.cbs.dtu.dk/services/TargetP/) and PREDOTAR (http://urgi.versailles.inra.fr/predotar/predotar.html) software. The prediction of a residue to belong to a transmembrane helix was realized using the TMHMM server (http://www.cbs.dtu.dk/services/TMHMM/).

YFP- and GFP-fused protein expression plasmids

For construction of the TDC-GFP and GFP-TDC expression vectors, the full-length ORF of TDC (GenBank M25151) was amplified by PCR using primers TDC-GFP-for and TDC-GFPrev (Table 2), which have been designed to eliminate the termination codon and to introduce a *Spe*I restriction site at both cDNA extremities. The amplified cDNA was subsequently sequenced and cloned into the *Spe*I or *Nhe*I restriction site of pSCA-cassette GFPi [18] in frame with the 5′ or 3′ extremity of the coding sequence of GFP to express the TDC-GFP or GFP-TDC fusion proteins, respectively.

The LAMT-YFP and YFP-LAMT expression vectors were constructed after amplification of the coding sequence of LAMT (Genbank EU057974) with primers LAM-YFP-for and LAM-YFPrev (Table 2), allowing the addition of *Spe*I restriction sites at both the 5′ and 3′ extremity of the amplified sequence. After verification by sequencing, the LAMT cDNA was cloned either into the *Spe*I or *Nhe*I restriction site of pSCA-cassette YFPi [18] to generate LAMT-YFP or YFP-LAMT, respectively.

The transient expression of the SLS-GFP fusion protein and the two deleted versions of SLS-GFP were achieved using the pSCA-cassette GFPi vector. To construct the SLS-GFP expression vector, the full-length ORF of SLS (GenBank L10081) was amplified by PCR using primers SLS-S and SLS-AS (Table 2). For the thSLS-GFP expression vector, the coding sequence of the putative transmembrane helix (first 33 residues) was amplified with primers SLS-pep-for and SLS-pep-rev (Table 2). The ΔthSLS-GFP expression vector expressing a transmembrane helix-deleted version of SLS was constructed after amplification of the coding sequence of the remaining part of the protein (residues 34–524) using primers SLS-del-S and SLS-del-AS (Table 2), allowing the addition of an initiation codon before residue 34 of the deleted version of SLS. All these primers have been designed to eliminate the termination codon and to introduce *Bgl*II or *Spe*I restriction sites to the extremities of the cDNA. These cDNA were subsequently sequenced and cloned into the corresponding restriction sites of pSCA-cassette GFPi in frame with the 5′ extremity of the coding sequence of mGFP5* driven by the CamV35S promoter to express the fusion protein.

BiFC studies of TDC and LAMT oligomerization

For the analysis of oligomerization of TDC and LAMT, BiFC assays were conducted using the pSPYNE(R)173 and pSPYCE(MR) plasmids [45], which allow the expression of a protein fused to the C-terminus of the split-YFP fragments, and the pSCA-SPYNE173 and pSCA-SPYCE(M) plasmids [2] for the expression of fusion proteins with the split-YFP N-terminal end. For both TDC and LAMT, the cDNAs amplified using TDC-GFPfor and TDC-GFP or LAM-YFPfor and LAM-YFPrev (Table 2) were cloned *via Spe*I in frame with the 5′ or 3′ ends of the coding sequence of the N-terminal (YFP^N, amino acids 1–173) and C-terminal (YFP^C, amino acids 156–239) fragments of YFP. This led to the production of a set of four distinct fusion proteins for TDC and LAMT, with each type of fusion including YFP^N-LAMT, YFP^C-LAMT, LAMT-YFP^N and LAMT-YFP^C as described for LAMT.

Organelle markers

For the identification of the subcellular compartments that accumulate the fusion proteins, a set of organelle markers was used in co-transformation experiments with the TDC, LAMT and SLS constructs. The 'ER'-mcherry marker (CD3-960) [46] was obtained from the Arabidopsis Biological Resource Center (http://www.arabidopsis.org). The CFP-GUS and mcherry-GUS cytosolic markers, the CFP nucleocytosolic marker and the 'nucleus'-mcherry-GUS marker have been described previously [2,15].

Biolistic-mediated transient transformation of *C. roseus* suspension cells

Transient transformation of *C. roseus* cells was performed by particle bombardment with the Bio-Rad PDS1000/He system in accordance an optimized protocol of biolistic transformation that has been described previously [18], with adaptation for BiFC assays [2].

GFP imaging through epifluorescence microscopy

An Olympus BX51 epifluorescence microscope equipped with an Olympus DP71 digital camera (Olympus, Tokyo, Japan) and CELL*D imaging software (Soft Imaging System, Olympus, Rungis, France) were used for image capture of *C. roseus* cells expressing the GFP-,YFP-, CFP- and mcherry-fused proteins. The YFP fluorescence was visualized using a JP2 filter set (Chroma#31040, 500–520 nm excitation filter, 540–580 nm band pass emission filter; Chroma Technology Corp., Bellows Falls, VT, USA) and CFP fluorescence was recorded with the CFP filter set (Chroma#31044v2, 426–446 nm excitation filter, 460–500 nm band pass emission filter). The JP1 filter set (Chroma#31039, 460–480 nm excitation filter, 500–520 nm band pass emission filter) and the Texas Red filter (Olympus U-MWIY2, 545–580 nm excitation filter, 610 nm long pass emission filter) were used to visualize GFP and mcherry fluorescence, respectively. CELL*D imaging software was used for merging both false-coloured images.

Plasmid constructions and yeast two-hybrid interaction tests

The two-hybrid assays were performed by using a LexA DNA-binding domain encoding bait vector (pBTM116 referred as pLex) and a Gal4 activation domain encoding prey vector (pGADT7). After amplification using each combination of two yeast primers (Table 2), *BamH*I cloning was performed in both vectors. Co-transformant yeasts were selected onto leucine-trytophan lacking medium (–LW) for 4 days at 30 °C, then streaked onto leucine-trytophan-histidine lacking medium (–LWH) and grown for 4 days at 30 °C. As a result of weak autoactivation of hybrid proteins, 3-amino-1,2,4-triazole was supplemented to –LWH medium at a concentration of 5 mM. X-Gal assays were performed in accordance with the overlay method described previously [47]. Briefly, 10 mL of an X-Gal mixture containing agar (0.5%), phosphate buffer (0.25 M), SDS (0.1%) and X-Gal (0.04%) are poured directly onto the –LWH medium containing streaked positive yeasts. The blue colour is allowed to appear for 3 h at 30 °C.

Tissue fixation, embedding in paraffin and sectioning

RNase-free conditions were strictly observed for all steps. All glassware was baked for 8 h at 180 °C and nondisposable plasticwares were incubated for 10 min in an aqueous 3% H_2O_2 solution before washing in diethylpyrocarbonate-treated water. Leaves from mature *C. roseus* plants grown in green house were harvested in late spring/early summer, and young germinating seedlings were rapidly fixed in formalin/acetic acid/alcohol and embedded in Paraplast (Dominique Dutscher, Brumath, France) as described previously [12,17,48]. Serial sections (10 μm) were spread on silane-coated slides overnight at 40 °C, and paraffin was removed using xylene (twice for 15 min) before rehydration in an ethanol gradient series up to diethylpyrocarbonate-treated water.

In situ hybridization

The protocol used has been described previously [12,14,23]. Full-length *LAMT* cDNA amplified using primers LAM-YFPfor and LAM-YFPrev (Table 2) and cloned in pSC-A amp/kan (Agilent Technologies, Massy, France) was used for the synthesis of sense and anti-sense digoxigenin-labelled

RNA probes. For SLS, the previously described plasmid was used for the transcription of riboprobes [8]. After prehybridization, hybridization of the digoxigenin-labelled probes and washing, the riboprobes were immunodetected using a sheep anti-digoxigenin Fab fragments-alkaline phosphatase conjugate (Roche, Meylan, France), and the conjugates were visualized using after overnight incubation in nitro-blue tetrazolium chloride/5-bromo-4-chloro-3′-indolyphosphate *p*-toluidine salt chromogenic substrate.

Acknowledgements

This research was financially supported by the Ministère de l'Enseignement Supérieur et de la Recherche and the Ligue contre le cancer and by a grant from the University of Tours. We thank Professor Jörg Kudla (University of Münster, Germany) for providing us with the BiFC plasmids. We also thank Dr Andrew J. Simkin for careful revision of the manuscript, as well as two anonymous referees for their constructive comments.

References

1 Guirimand G, Courdavault V, St-Pierre B & Burlat V (2010) Biosynthesis and regulation of alkaloids. In *Plant Developmental Biology – Biotechnological Perspectives vol 2* (Pua EC & Davey M eds), pp. 139–160. Springer Verlag, Berlin Heidelberg.

2 Guirimand G, Courdavault V, Lanoue A, Mahroug S, Guihur A, Blanc N, Giglioli-Guivarc'h N, St-Pierre B & Burlat V (2010) Strictosidine activation in Apocynaceae: towards a 'nuclear time bomb'? *BMC Plant Biol* **10**, 182.

3 Roepke J, Salim V, Wu M, Thamm AMK, Murata J, Ploss K, Boland W & De Luca V (2010) Vinca drug components accumulate exclusively in leaf exudates of Madagascar periwinkle. *Proc Natl Acad Sci USA* **107**, 15287–15292.

4 Ziegler J & Facchini PJ (2008) Alkaloid biosynthesis: metabolism and trafficking. *Annu Rev Plant Biol* **59**, 735–769.

5 De Luca V, Marineau C & Brisson N (1989) Molecular cloning and analysis of cDNA encoding a plant tryptophan decarboxylase – comparison with animal dopa decarboxylases. *Proc Natl Acad Sci USA* **86**, 2582–2586.

6 Contin A, van der Heijden R, Lefeber AWM & Verpoorte R (1998) The iridoid glucoside secologanin is derived from the novel triose phosphate/pyruvate pathway in a *Catharanthus roseus* cell culture. *FEBS Lett* **434**, 413–416.

7 Collu G, Unver N, Peltenburg-Looman AMG, van der Heijden R, Verpoorte R & Memelink J (2001) Geraniol 10-hydroxylase, a cytochrome P450 enzyme involved in terpenoid indole alkaloid biosynthesis. *FEBS Lett* **508**, 215–220.

8 Irmler S, Schröder G, St-Pierre B, Crouch NP, Hotze M, Schmidt J, Strack D, Matern U & Schröder J (2000) Indole alkaloid biosynthesis in *Catharanthus roseus*: new enzyme activities and identification of cytochrome P450 CYP72A1 as secologanin synthase. *Plant J* **24**, 797–804.

9 Murata J, Roepke J, Gordon H & De Luca V (2008) The leaf epidermome of *Catharanthus roseus* reveals its biochemical specialization. *Plant Cell* **20**, 524–542.

10 de Waal A, Meijer AH & Verpoorte R (1995) Strictosidine synthase from *Catharanthus roseus* – Purification and characterization of multiple forms. *Biochem J* **306**, 571–580.

11 Geerlings A, Ibanez MML, Memelink J, van der Heijden R & Verpoorte R (2000) Molecular cloning and analysis of strictosidine beta-d-glucosidase, an enzyme in terpenoid indole alkaloid biosynthesis in *Catharanthus roseus*. *J Biol Chem* **275**, 3051–3056.

12 Burlat V, Oudin A, Courtois M, Rideau M & St-Pierre B (2004) Co-expression of three MEP pathway genes and geraniol 10-hydroxylase in internal phloem parenchyma of *Catharanthus roseus* implicates multicellular translocation of intermediates during the biosynthesis of monoterpene indole alkaloids and isoprenoid-derived primary metabolites. *Plant J* **38**, 131–141.

13 Courdavault V, Burlat V, St-Pierre B & Giglioli-Guivarc'h N (2005) Characterisation of CaaX-prenyltransferases in *Catharanthus roseus*: relationships with the expression of genes involved in the early stages of monoterpenoid biosynthetic pathway. *Plant Sci* **168**, 1097–1107.

14 Oudin A, Mahroug S, Courdavault V, Hervouet N, Zelwer C, Rodríguez-Concepción M, St-Pierre B & Burlat V (2007) Spatial distribution and hormonal regulation of gene products from methyl erythritol phosphate and monoterpene-secoiridoid pathways in *Catharanthus roseus*. *Plant Mol Biol* **65**, 13–30.

15 Guirimand G, Guihur A, Poutrain P, Héricourt F, Mahroug S, St-Pierre B, Burlat V & Courdavault V(2010) Spatial organization of the vindoline biosynthetic pathway in *Catharanthus roseus*. *J Plant Physiol* doi:10.1016/j.jplph.2010.08.018, in press.

16 Murata J & De Luca V (2005) Localization of tabersonine 16-hydroxylase and 16-OH tabersonine-16-O-methyltransferase to leaf epidermal cells defines them as a major site of precursor biosynthesis in the vindoline pathway in *Catharanthus roseus*. *Plant J* **44**, 581–594.

17 St-Pierre B, Vázquez-Flota FA & De Luca V (1999) Multicellular compartmentation of *Catharanthus roseus* alkaloid biosynthesis predicts intercellular translocation of a pathway intermediate. *Plant Cell* **11**, 887–900.

18 Guirimand G, Burlat V, Oudin A, Lanoue A, St-Pierre B & Courdavault V (2009) Optimization of the transient

transformation of *Catharanthus roseus* cells by particle bombardment and its application to the subcellular localization of hydroxymethylbutenyl 4-diphosphate synthase and geraniol 10-hydroxylase. *Plant Cell Rep* **28**, 1215–1234.
19 Hedhili S, Courdavault V, Giglioli-Guivarc'h N & Gantet P (2007) Regulation of the terpene moiety biosynthesis of *Catharanthus roseus* terpene indole alkaloids. *Phytochem Rev* **6**, 341–351.
20 St-Pierre B & De Luca V (1995) A cytochrome P450 monooxygenase catalyses the first step in the conversion of tabersonine to vindoline in *Catharanthus roseus*. *Plant Physiol* **109**, 131–139.
21 Kutchan TM (2005) A role for intra- and intercellular translocation in natural product biosynthesis. *Curr Opin Plant Biol* **8**, 292–300.
22 Mahroug S, Burlat V & St-Pierre B (2007) Cellular and sub-cellular organisation of the monoterpenoid indole alkaloid pathway in *Catharanthus roseus*. *Phytochem Rev* **6**, 363–381.
23 Mahroug S, Courdavault V, Thiersault M, St-Pierre B & Burlat V (2006) Epidermis is a pivotal site of at least four secondary metabolic pathways in *Catharanthus roseus* aerial organs. *Planta* **223**, 1191–1200.
24 Stevens LH, Blom TJM & Verpoorte R (1993) Subcellular localization of tryptophan decarboxylase, strictosidine synthase and strictosidine glucosidase in suspension-cultured cells of *Catharanthus roseus* and *Tabernaemontana divaricata*. *Plant Cell Rep* **12**, 573–576.
25 Moreno-Valenzuela OA, Minero-García Y, Brito-Argáez L, Carbajal-Mora E, Echeverría O, Vázquez-Nin G & Loyola-Vargas VM (2003) Immunocytolocalization of tryptophan decarboxylase in *Catharanthus roseus* hairy roots. *Mol Biotechnol* **23**, 11–18.
26 Goddijn OJM, Lohman FP, de Kam RJ, Schilperoort RA & Hoge JHC (1994) Nucleotide sequence of the tryptophan decarboxylase gene of *Catharanthus roseus* and expression of tdc-gusA gene fusions in *Nicotiana tabacum*. *Mol Gen Genet* **242**, 217–225.
27 Meijer AH, Verpoorte R & Hoge JHC (1993) Regulation of enzymes and genes involved in terpenoid indole alkaloid biosynthesis in *Catharanthus roseus*. *J Plant Res*, **3**, 145–164.
28 Fernandez JA, Owen TG, Kurz WGW & De Luca V (1989) Immunological detection and quantitation of tryptophan decarboxylase in developing *Catharanthus roseus* seedlings. *Plant Physiol* **91**, 79–84.
29 Islas-Flores I, Moreno-Valenzuela O, Minero-García Y, Loyola-Vargas VM & Miranda-Ham Mde L (2002) Tryptophan decarboxylase from transformed roots of *Catharanthus roseus*. *Mol Biotechnol* **21**, 211–216.
30 Noé W, Mollenschott C & Berlin J (1984) Tryptophan decarboxylase from *Catharanthus roseus* cell suspension cultures – purification, molecular and kinetic data of the homogeneous protein. *Plant Mol Biol* **3**, 281–288.
31 Pennings EJM, Groen BW, Duine JA & Verpoorte R (1989) Tryptophan decarboxylase from *Catharanthus roseus* is a pyridoxo-quinoprotein. *FEBS Lett* **255**, 97–100.
32 Wang RW & Brattain MG (2007) The maximal size of protein to diffuse through the nuclear pore is larger than 60 kDa. *FEBS Lett* **581**, 3164–3170.
33 Zubieta C, He XZ, Dixon RA & Noel JP (2001) Structures of two natural product methyltransferases reveal the basis for substrate specificity in plant O-methyltransferases. *Nat Struct Biol* **8**, 271–279.
34 Zubieta C, Kota P, Ferrer JL, Dixon RA & Noel JP (2002) Structural basis for the modulation of lignin monomer methylation by caffeic acid/5-hydroxyferulic acid 3/5-O-methyltransferase. *Plant Cell* **14**, 1265–1277.
35 Zubieta C, Ross JR, Koscheski P, Yang Y, Pichersky E & Noel JP (2003) Structural basis for substrate recognition in the salicylic acid carboxyl methyltransferase family. *Plant Cell* **15**, 1704–1716.
36 Contin A, van der Heijden R, ten Hoopen HJG & Verpoorte R (1998) The inoculum size triggers tryptamine or secologanin biosynthesis in a *Catharanthus roseus* cell culture. *Plant Sci* **139**, 205–211.
37 Contin A, van der Heijden R & Verpoorte R (1999) Accumulation of loganin and secologanin in vacuoles from suspension cultured *Catharanthus roseus* cells. *Plant Sci* **147**, 177–183.
38 Yamazaki S, Sato K, Suhara K, Sakaguchi M, Mihara K & Omura T (1993) Importance of the proline-rich region following signal-anchor sequence in the formation of correct conformation of microsomal cytochrome P450s. *J Biochem* **114**, 652–657.
39 Schuler MA & Werck-Reichhart D (2003) Functional genomics of P450s. *Annu Rev Plant Biol* **54**, 629–667.
40 Snapp EL, Hegde RS, Francolini M, Lombardo F, Colobo S, Pedrazzini E, Borgese N & Lippincott-Schwartz J (2003) Formation of stacked ER cisternae by low affinity protein interactions. *J Cell Biol* **163**, 257–269.
41 Roytrakul S & Verpoorte R (2007) Role of vacuolar transporter proteins in plant secondary metabolism: *Catharanthus roseus* cell culture. *Phytochem Rev* **6**, 383–396.
42 Sakai K, Shitan N, Sato F, Ueda K & Yazaki K (2002) Characterization of berberine transport into *Coptis japonica* cells and the involvement of ABC protein. *J Exp Bot* **53**, 1879–1886.
43 Shitan N, Bazin I, Dan K, Obata K, Kigawa K, Ueda K, Sato F, Forestier C & Yazaki K (2003) Involvement of CjMDR1, a plant multidrug-resistance-type ATP-binding cassette protein, in alkaloid transport in *Coptis japonica*. *Proc Natl Acad Sci USA* **100**, 751–756.

44 Courdavault V, Thiersault M, Courtois M, Gantet P, Oudin A, Doireau P, St-Pierre B & Giglioli-Guivarc'h N (2005) CaaX-prenyltransferases are essential for expression of genes involvedin the early stages of monoterpenoid biosynthetic pathway in *Catharanthus roseus* cells. *Plant Mol Biol* **57**, 855–870.
45 Waadt R, Schmidt LK, Lohse M, Hashimoto K, Bock R & Kudla J (2008) Multicolor bimolecular fluorescence complementation reveals simultaneous formation of alternative CBL/CIPK complexes in planta. *Plant J* **56**, 505–516.
46 Nelson BK, Cai X & Nebenführ A (2007) A multicolored set of *in vivo* organelle markers for co-localization studies in Arabidopsis and other plants. *Plant J* **51**, 1126–1136.
47 Fromont-Racine M, Rain JC & Legrain P (1997) Toward a functional analysis of the yeast genome through exhaustive two-hybrid screens. *Nat Genet* **16**, 277–282.
48 Poutrain P, Guirimand G, Mahroug S, Burlat V, Melin C, Ginis O, Oudin A, Giglioli-Guivarc'h N, Pichon O & Courdavault V (2011) Molecular cloning and characterisation of two calmodulin isoforms of the Madagascar periwinkle *Catharanthus roseus*. *Plant Biol* **13**, 36–41.